OBSERVATIONS OF LOVE WAVES FROM THE HUMBLE REDWOOD EXPLOSIONS WITH IMPLICATIONS FOR *P/S* RATIOS AT LOCAL DISTANCES

Mark Leidig[1], Robert E. Reinke[2], Jessie L. Bonner[1], Howard J. Patton[3], Xiaoning (David) Yang[3], William R. Walter[4], Sean R. Ford[4], Bill Foxall[4], and Brian W. Stump[5]

Weston Geophysical Corporation[1], Defense Threat Reduction Agency[2], Los Alamos National Laboratory[3], Lawrence Livermore National Laboratory[4], and Southern Methodist University[5]

Sponsored by the National Nuclear Security Administration

Award Nos. DE-AC52-08NA28655[1,5], DE-AC52-06NA25396[3], and DE-AC52-07NA27344[4]
Proposal No. BAA08-97

ABSTRACT

The ratio of 6-8 Hz *P/S* energy is a robust discriminant between earthquakes and explosions at regional distances (e.g., Taylor et al., 1989; Walter et al., 1995; Hartse et al., 1997; Pasyanos et al., 2009). We have examined the *P/S* discriminant at regional and local distances for simultaneously-detonated chemical explosions conducted for the Non-Proliferation Experiment (NPE), Source Phenomenology Experiments in Arizona (SPE Black Mesa and Morenci), Alaska Frozen Rock Experiments (FRE Frozen and Unfrozen), and the New England Damage Experiment (NEDE). These shots were conducted at various scaled depths of burial in lithology ranging from granite to alluvium. Several of these datasets have delay-fired mining explosions detonated in close proximity to the dedicated shots for comparison. During the past year, we have added additional datasets to our analysis of *P/S* ratios from explosions: HUMBLE REDWOOD (HR) I and II.

The HR I and II experiments (Foxall et al., 2008,2010) provide a unique opportunity to study local phase generation, in particular *S*-waves, from above- and below-ground explosions. We have identified *P*-waves, higher and fundamental-mode Rayleigh (*Rg*) waves, and Love (specifically *SH,* the horizontally polarized shear wave) waves from 656 kg ANFO explosions detonated above and in alluvium in the Albuquerque Basin, New Mexico. Identification of *P* and *Rg* was relatively simple based on arrival times and rectilinear and retrograde elliptical particle motion, respectively. Identification of higher mode Rayleigh waves required particle motion (prograde elliptical) and synthetic modeling. The candidate *SH* arrivals from the above-ground shots are difficult to positively identify as Love waves due to small amplitudes and complex particle motion. Conversely, the *SH* arrivals for most of the below-ground explosions are positively identified as Love waves with transverse particle motion and group velocity dispersion curves that match the theoretical curves for a local velocity model based only on *Rg*. We explore possible sources for Love wave generation from these explosions ranging from asymmetries in the source region to damage/crack generation in low-strength media.

We compared *P/S* ratios for the HR events and 13 earthquakes within a one degree radius of the HR test site. We also compared the *P/S* ratios for the HR events to the SPE, FRE, and NEDE results. The HR *P/S* ratios range from 0.1 to 1 at frequencies less than 8 Hz and are much greater than one between 8-20 Hz. The earthquake *P/S* ratios do not vary much with either distance or frequency and generally lie between 0.1 and 1. Thus, the HR explosions separate significantly from the nearby earthquakes at 8-16 Hz, but overall the *P/S* ratio discriminant performs poorly below 8 Hz. Other local explosion events (e.g., NEDE) do not discriminate from earthquakes at all below 16 Hz. Local to near-regional distance *P/S* discrimination is made more complex because the seismic waves spend a greater percentage of their travel path in the shallow crust where the seismic structure, velocity, and attenuation vary significantly. Initial research indicates that network averaged *P/S* ratios improve the event discrimination reliability.

Report Documentation Page

Form Approved
OMB No. 0704-0188

1. REPORT DATE	2. REPORT TYPE	3. DATES COVERED
SEP 2011		**00-00-2011 to 00-00-2011**

4. TITLE AND SUBTITLE	5a. CONTRACT NUMBER
Observations of Love Waves from the HUMBLE REDWOOD Explosions with Implications for P/S Ratios at Local Distances	5b. GRANT NUMBER
	5c. PROGRAM ELEMENT NUMBER
6. AUTHOR(S)	5d. PROJECT NUMBER
	5e. TASK NUMBER
	5f. WORK UNIT NUMBER
7. PERFORMING ORGANIZATION NAME(S) AND ADDRESS(ES) **Weston Geophysical Corporation,181 Bedford Street, Suite 1,Lexington,MA,02420**	8. PERFORMING ORGANIZATION REPORT NUMBER
9. SPONSORING/MONITORING AGENCY NAME(S) AND ADDRESS(ES)	10. SPONSOR/MONITOR'S ACRONYM(S)
	11. SPONSOR/MONITOR'S REPORT NUMBER(S)

12. DISTRIBUTION/AVAILABILITY STATEMENT

Approved for public release; distribution unlimited

13. SUPPLEMENTARY NOTES

Published in the Proceedings of the 2011 Monitoring Research Review - Ground-Based Nuclear Explosion Monitoring Technologies, 13-15 September 2011, Tucson, AZ. Volume I. Sponsored by the Air Force Research Laboratory (AFRL) and the National Nuclear Security Administration (NNSA). U.S. Government or Federal Rights License

14. ABSTRACT

The ratio of 6-8 Hz P/S energy is a robust discriminant between earthquakes and explosions at regional distances (e.g., Taylor et al., 1989; Walter et al., 1995; Hartse et al., 1997; Pasyanos et al., 2009). We have examined the P/S discriminant at regional and local distances for simultaneously-detonated chemical explosions conducted for the Non-Proliferation Experiment (NPE), Source Phenomenology Experiments in Arizona (SPE Black Mesa and Morenci), Alaska Frozen Rock Experiments (FRE Frozen and Unfrozen) and the New England Damage Experiment (NEDE). These shots were conducted at various scaled depths of burial in lithology ranging from granite to alluvium. Several of these datasets have delay-fired mining explosions detonated in close proximity to the dedicated shots for comparison. During the past year, we have added additional datasets to our analysis of P/S ratios from explosions: HUMBLE REDWOOD (HR) I and II. The HR I and II experiments (Foxall et al., 2008,2010) provide a unique opportunity to study local phase generation, in particular S-waves, from above- and below-ground explosions. We have identified P-waves higher and fundamental-mode Rayleigh (Rg) waves, and Love (specifically SH, the horizontally polarized shear wave) waves from 656 kg ANFO explosions detonated above and in alluvium in the Albuquerque Basin, New Mexico. Identification of P and Rg was relatively simple based on arrival times and rectilinear and retrograde elliptical particle motion, respectively. Identification of higher mode Rayleigh waves required particle motion (prograde elliptical) and synthetic modeling. The candidate SH arrivals from the above-ground shots are difficult to positively identify as Love waves due to small amplitudes and complex particle motion. Conversely, the SH arrivals for most of the below-ground explosions are positively identified as Love waves with transverse particle motion and group velocity dispersion curves that match the theoretical curves for a local velocity model based only on Rg. We explore possible sources for Love wave generation from these explosions ranging from asymmetries in the source region to damage/crack generation in low-strength media. We compared P/S ratios for the HR events and 13 earthquakes within a one degree radius of the HR test site. We also compared the P/S ratios for the HR events to the SPE, FRE, and NEDE results. The HR P/S ratios range from 0.1 to 1 at frequencies less than 8 Hz and are much greater than one between 8-20 Hz. The earthquake P/S ratios do not vary much with either distance or frequency and generally lie between 0.1 and 1. Thus, the HR explosions separate significantly from the nearby earthquakes at 8-16 Hz, but overall the P/S ratio discriminant performs poorly below 8 Hz. Other local explosion events (e.g., NEDE) do not discriminate from earthquakes at all below 16 Hz. Local to near-regional distance P/S discrimination is

15. SUBJECT TERMS

16. SECURITY CLASSIFICATION OF:			17. LIMITATION OF ABSTRACT	18. NUMBER OF PAGES	19a. NAME OF RESPONSIBLE PERSON
a. REPORT	b. ABSTRACT	c. THIS PAGE			
unclassified	**unclassified**	**unclassified**	**Same as Report (SAR)**	**10**	

OBJECTIVES

We continue to study local-to-regional phase generation from explosions. Two experimental datasets recently collected in Albuquerque, New Mexico have provided an opportunity to study *S*-wave generation from explosions. These incredible datasets allow comparing and contrasting seismic phases, including *S*-waves, from co-located explosions above and below ground. In this paper, we differentiate the seismic phases generated by these explosions, with a primary focus on the *S*-waves. We identify the phases using particle motion analyses and waveform modeling, and then quantify differences between the *S*-phases as a function of height of burst (HOB) or depth of burial (DOB). Finally, we estimate *P/S* ratios for the explosions and nearby earthquakes.

RESEARCH ACCOMPLISHED

The HUMBLE REDWOOD Experiments

In 2007 and 2009, the Defense Threat Reduction Agency and the Department of Energy (Lawrence Livermore National Laboratory) detonated two series of above- and below-ground explosions known as HUMBLE REDWOOD I and II (HRI and HRII). HRI and HRII were carried out to advance the understanding of partial seismic coupling for shallow explosions (Foxall et al., 2008, 2010). The HRI experiment was comprised of seven 1450-lb ANFO charges detonated at various HOBs and DOBs. HRII included three additional 1450-lb detonations as well as three blind yield and DOB shots. Both sets of experiments were conducted in and above the dry alluvium of Kirtland AFB, NM near the eastern margin of the Albuquerque Basin, and were recorded by extensive local seismic and acoustic networks. Crater parameters (Lenox et al., 2008) and permanent near-source surface displacements were derived using digital photogrammetric techniques. The complete HUMBLE REDWOOD data set ranges from fully contained to no-crater height of burst shots and covers almost an order of magnitude in explosive yield.

For this paper, we focus our analysis on the waveforms from the ten 1450-lb HRI and HRII explosions recorded at stations W5 (34.9566N 106.5668W) and W4 (34.9572N 106.5568W) located 1.9 km and 1 km west of ground zero (GZ), respectively. Both sites consisted of a Guralp 40T three-component (3C) seismometer operating at 500 samples/sec and buried just below the surface. Figure 1 shows the vertical, radial, and transverse components for all ten shots recorded at W5. The data are plotted as a function of the HOB, with negative values referring to the buried explosions. The shots range from HRI-A, which was detonated at 5 meters above the surface on a wooden platform to HRII-3, which was detonated 10 meters below the surface. The shape of the charges was cylindrical with the same dimensions for all ten 1450-lb explosions.

The vertical and radial data (Figure 1) provide a glimpse at the uniqueness and quality of this dataset as the waveforms from the different explosions are remarkably similar. The only differences in these waveforms are the amplitudes—the below-ground explosions couple better and have larger amplitudes than the atmospheric shots—and the existence of the air-coupled Rayleigh (AR) waves, which are most prominent on the above ground or partially-coupled explosions. Murphy et al. (1982) observed no differences for amplitudes of Rayleigh waves induced by atmospheric explosions for scaled HOBs < 500 m/kt$^{1/3}$. For these explosions, which had scaled HOBs < 50 m/kt$^{1/3}$, we note little, if any, amplitude or phase differences between all observed phases on the four above ground explosions.

Phase Identification

***P*-waves.** We observe five prominent arrivals on the W5 seismograms (Figure 1). The first is the *P*-wave, which arrives ~1 second after the origin of the blast at a group velocity of ~2 km/sec. The hodograms (Figure 1) show all 10 shots produced *P*-waves at W5 with similar rectilinear particle motion away from the source. The larger vertical component (Z) of motion than radial component (R) suggests these are turning rays. The subsurface of the Albuquerque Basin near GZ consists of dry alluvium, with *P*-wave velocities less than 1 km/sec, underlain by faster velocity rocks (> 2.5 km/sec). The *P*-waves at W5 are

turning in this faster material. The *P*-waves are not the focus of this paper, but are being studied in detail by Marrs et al., 2011.

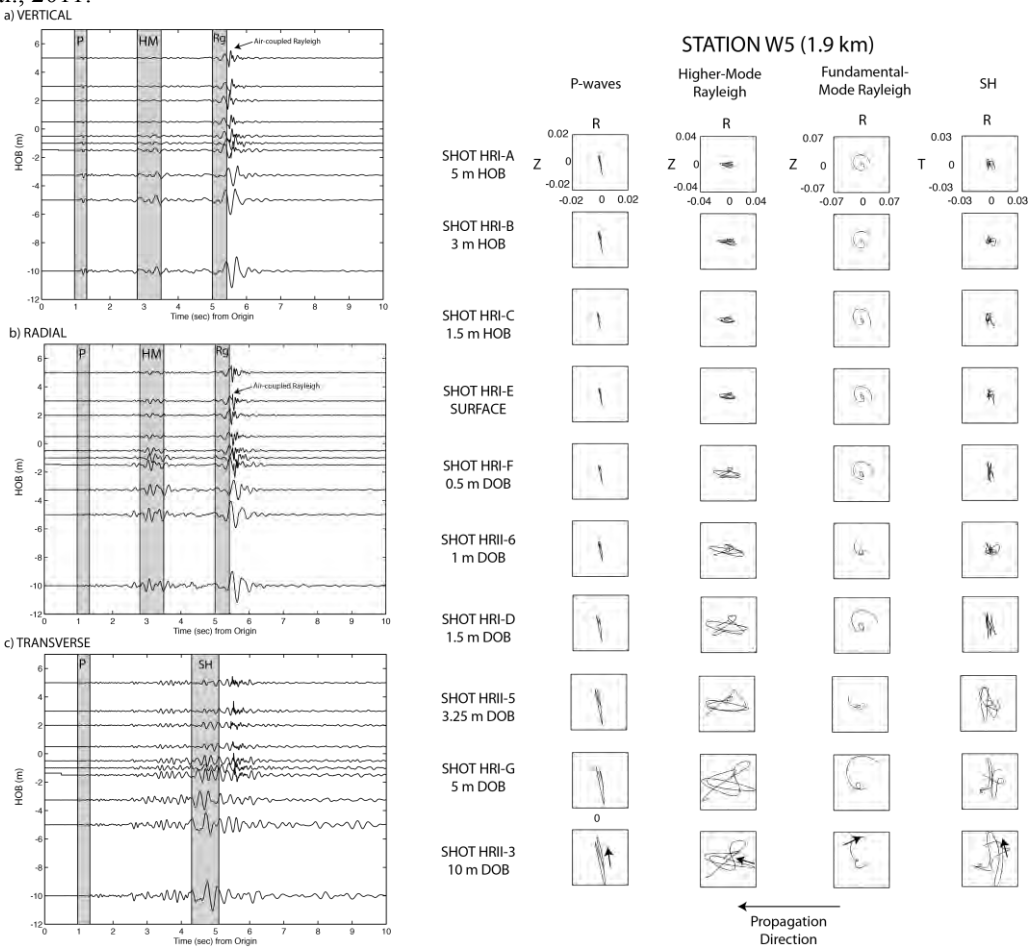

Figure 1. (Left) Vertical (a), radial (b), and transverse (c) component waveforms for HRI and HRII explosions recorded at station W5. The waveforms are plotted as a function of their height of burst (HOB) in meters. The shaded regions represent *P*, higher-mode Rayleigh waves (HM), fundamental-mode Rayleigh waves (*Rg*) and shear waves (*SH*). (Right) Particle motion hodograms for four different arrivals recorded at station W5 from ten 1450-lb explosions at different HOB/DOBs.

Fundamental Mode Rayleigh (*Rg*). Perhaps the easiest phase to identify on the 3C recordings at W5 is the fundamental mode (FM) Rayleigh waves, often referred to as *Rg*. For shallow explosions and earthquakes, *Rg* is often the largest seismic arrival at local distances (e.g., < 100 km), and that is the case for the HUMBLE REDWOOD explosions recorded at most stations west of GZ, including W5. *Rg* is rapidly scattered to the east of GZ by a normal fault creating complex seismograms with difficult phase identification. Because the *Rg* is traveling in the dry, air-filled alluvium at velocities near the speed of sound, it is imprinted with the air-coupled Rayleigh-waves from the passage of the acoustic pressure front (which is the third of five phases identified on these seismic recordings). When windowing the *Rg* for particle motion analysis, we ended the window prior to the AR. The hodograms (Figure 1) show the *Rg* has retrograde elliptical particle motion. There is essentially no difference in the amplitudes and particle motion for *Rg* for the explosions at the surface and above. We observed larger *Rg* amplitudes for the buried explosions with slightly more complicated retrograde elliptical particle motion.

Higher-mode Rayleigh. The fourth seismic phase identified is higher-mode (HM) Rayleigh; however, identification of the phase was not immediate. Because the phase arrives midway between *P* and *Rg* —at

velocities less than ~0.75 km/sec—and appears as an isolated wave packet, the gut reaction is to label the phase as direct *S*-waves. But particle motion analysis provided no dominant *SH* polarized motion. Instead, the phase exhibited prograde elliptical motion (Figure 1) with group velocity dispersion. Reinke (1978) and Reamer and Stump (1992) identified similar large amplitude wave packets with prograde elliptical particle motion in alluvial basins in southern New Mexico and Arizona as HM Rayleigh waves. Thus we preliminarily identified this fourth phase as HM Rayleigh waves.

We attempted to confirm this phase designation using synthetics. As part of earlier work on the HRI dataset, we developed a velocity and attenuation model for the HR test site. The velocity model was initially developed using trial and error attempts to fit a velocity structure to observed *Rg* group velocity dispersion at station W2 (34.9663N 106.6117W), which was located 6 km west of GZ. After an initial velocity model was defined, it was refined using a linearized inversion technique (Herrmann, 2010). The attenuation structure was added later by incorporating amplitude decay data from linear profiles of short-period geophones deployed for the explosions. We generated modal summation synthetics (Herrmann, 2010) with and without higher modes (Figure 2) using the inverted model. The synthetics with fundamental and multiple higher modes provide a good match to the observed data at station W5. We note that only FM Rayleigh waves, recorded at stations other than W5, were used to develop the velocity model.

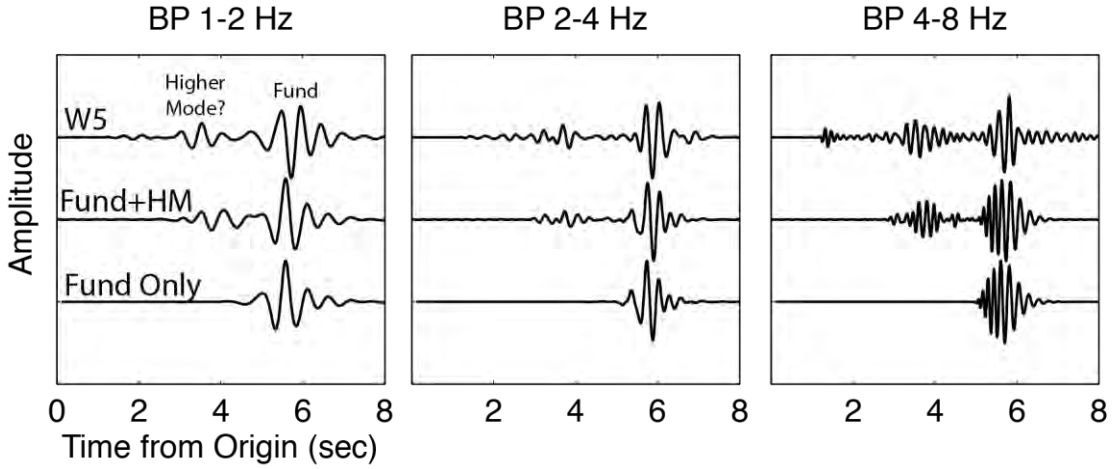

Figure 2. Synthetic modeling aids in the identification of the HM Rayleigh waves. Shown in each filter panel is the observed vertical component waveform, synthetics with the first 20 surface wave modes, and then the FM only synthetic. The data and synthetics were filtered at 1 to 2 Hz (left), 2 to 4 Hz (middle), and 4 to 8 Hz (right).

***S*-waves.** The fifth seismic arrival is observed only on the transverse components (Figure 1c). The particle motion on the above-ground shots is difficult to interpret due to small amplitudes on all three components in the phase window. However, horizontally-polarized ground motion is easily identified for the buried shots, with the exception of the 1 m DOB HRII-6. We identify this phase with transverse motion as an *SH*-wave.

To further aid in the interpretation of these *SH*-waves, we present Figure 3 which provides a more detailed view of the transverse components for W5 and W4. We introduce W4 to show the characteristics of the *SH* arrivals were not unique to a single station. W4 had very similar particle motion results as W5. For the previously-identified phases (e.g., *P*, HM, and FM Rayleigh), the primary difference between the above- and below-ground shots was amplitude. The amplitudes of the above ground shots and the 0.5 m DOB shot were approximately equivalent, while the below ground phase amplitudes increased with DOB due to enhanced seismic coupling. The peaks and troughs were ~~in~~ phase" and independent of DOB/HOB. This is not the case for the *SH*-waves, which have complex wave trains, variable arrival times, and amplitudes that do not increase simply with increasing DOB.

Further study of the *SH* phase shows it is dispersed. We applied the Multiple Filter Analysis technique (MFA; Dziewonski et al., 1969; Herrmann et al., 2010) to the 10 meter DOB shot, and the contoured

envelopes are shown in Figure 4a,b. The MFA results for the transverse component show a normally dispersed signal at periods between 0.2 and 1 sec at group velocities of 0.39 to 0.47 km/sec. The arrival has a peak amplitude (red contours) at 0.4 seconds (2.5 Hz). For comparison, the MFA of the vertical component (Figure 4b) shows the normally dispersed *Rg* at slower velocities. The dispersion ranges from 0.34 km/sec at 0.14 sec period (7 Hz) to 0.43 km/sec at 1.2 sec period. The HM Rayleigh is also observed on the MFA of the vertical component at periods between 0.2 and 0.7 sec and velocities of 0.55 to 0.7 km/sec.

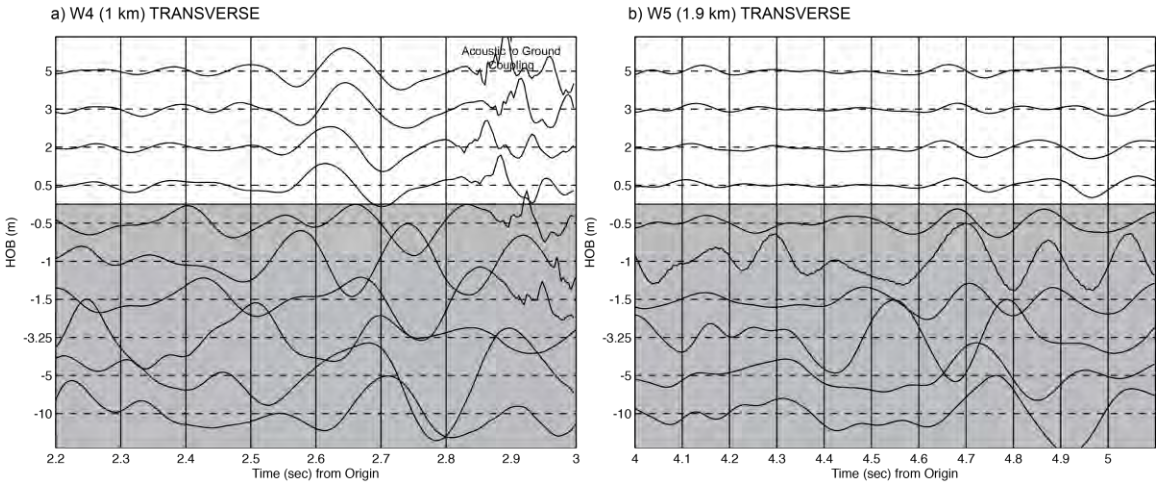

Figure 3. Transverse components for stations a) W4 and b) W5 highlighting the differences between the above- and below-ground (shaded region) explosions. Vertical lines are drawn every 0.1 seconds.

The MFA for the 5 meter HOB shot (Figure 4c,d) is slightly more complex. First, the largest amplitudes on both the transverse and vertical MFA plots are from the AR waves, which produce peak amplitudes on both MFAs at 0.25 seconds period and at 0.35 km/sec group velocity. At periods greater than 0.4 seconds, the effect of the air-coupled Rayleigh diminishes, and the *Rg* dispersion curve is easily identified on the vertical-component MFA. There also appears to be a possible *SH* arrival (labeled SH?) that has slightly higher group velocities than the *SH* observed for the 10 m DOB shot.

We completed similar MFA analyses on all 10 HRI and HRII recordings at W5 and extracted the FM and HM Rayleigh and *SH* dispersion curves (Figure 5a,b) and spectral amplitudes (Figure 5c,d). The dispersion curves for the FM and HM Rayleigh show minimal scatter. This is quite remarkable considering that for the shallow and above-ground explosions, the FM Rayleigh is contaminated by the AR. That contamination is evident in the spectral amplitudes as the FM Rayleigh (Figure 5c) for the above-ground explosions have different high-frequency roll off than the buried explosions. We measure about an order-of-magnitude difference in the spectral amplitudes for FM and HM Rayleigh between the shots at 5 m HOB and 10 m DOB. Also noted is that the *Rg* corner frequency decreases with increasing DOB, although the AR effects make the corner frequency shift in Figure 5c appear larger than it actually is.

We observed slightly more scatter in the *SH* dispersion curves (Figure 5b) for the 10 explosions at W5. These results show that only the deepest shots (>5 m DOB) generated *SH* waves across the entire band of 0.2 to 1 sec period. Also, the dispersion curves bifurcate at 0.8 sec period, with the two deepest shots having slower velocities than the shallow- and above-ground shots. The spectral amplitudes for the *SH* phase fall into three groups. First, the above ground explosions have *SH* spectral amplitudes that are small and overlay one another. The deepest (>5 m DOB) explosions have *SH* spectral amplitudes that are significantly larger than the above ground candidate *SH* phase. In fact, these *SH* phases from the deepest shots have amplitudes equivalent to the FM Rayleigh observed from the shallow (<5 m DOB) explosions. Finally, the shallow buried explosions (< 5 m DOB) have *SH* spectral levels somewhere in between the

above ground and deepest shots and exhibit variable spectral shapes due to spectral holes in the MFA analysis that complicates the interpretation.

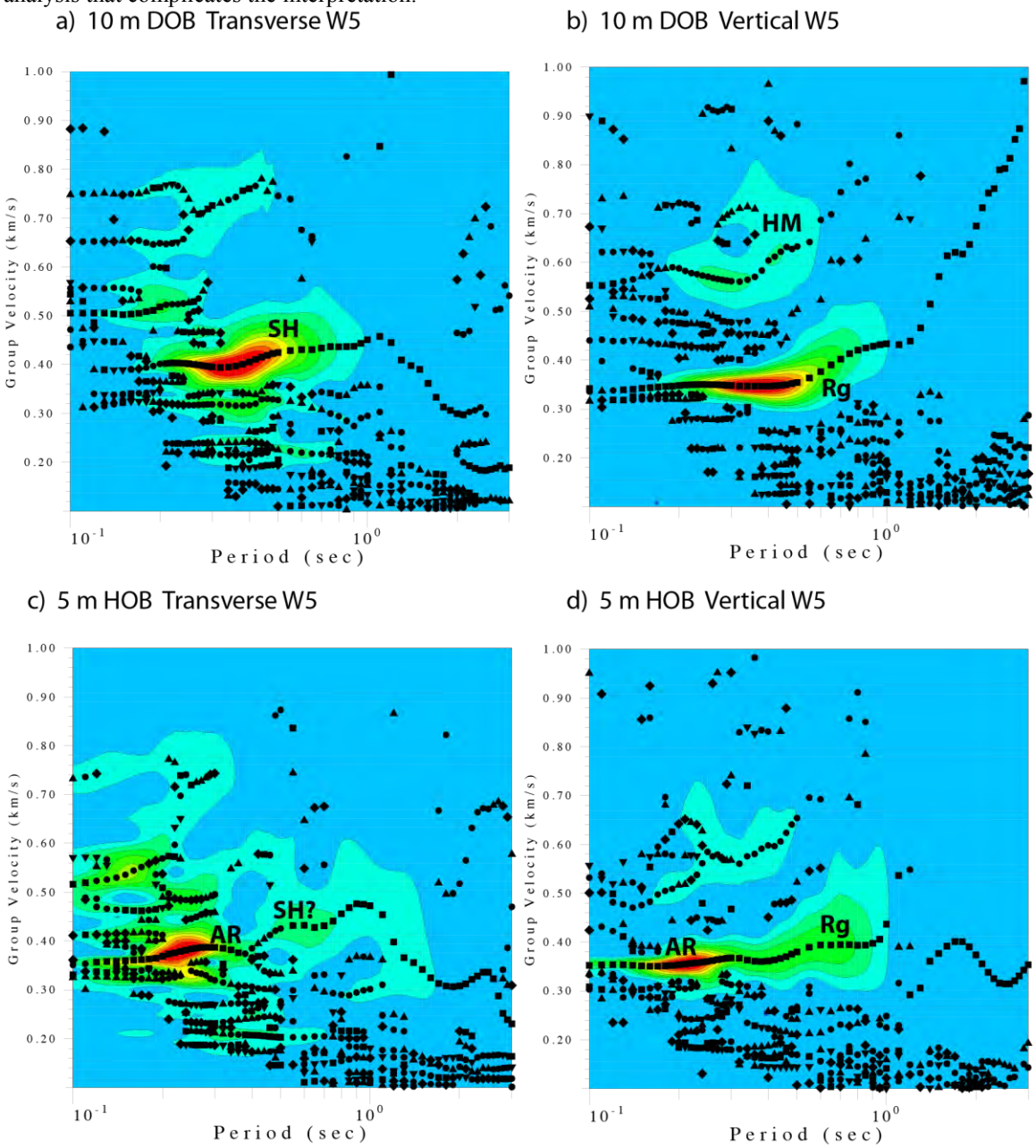

Figure 4. Multiple filter analysis technique (MFA) applied to the a) transverse and b) vertical component recordings for the 10 m DOB shot. The data are filtered at each period, and the resulting enveloped is contoured. Warm colors represent the largest amplitudes, which are often surface waves. Also shown is the MFA of the c) transverse and d) vertical components for the 5 m HOB shot.

Theoretical dispersion curves for our preferred velocity model were generated and plotted in Figures 5a, b. The curves match the observed FM and HM Rayleigh data quite well, especially considering that the model was developed using FM records only at other stations. The match between the theoretical and observed *SH* dispersion curves is acceptable, although the observed dispersion is slightly faster than the theoretical. The predicted Love wave dispersion provides a better fit to the dispersion curves for the deepest (> 5 m DOB)

explosions. It is interesting that the observed *SH* and FM Rayleigh group velocities are similar at periods between 0.5 to 0.8 seconds. This is predicted by the model, which predicts the Love waves to have group velocities slower than the FM Rayleigh at some periods. Based on the dispersion and particle motion results, we believe that the HRI and HRII explosions generated Love waves at the source.

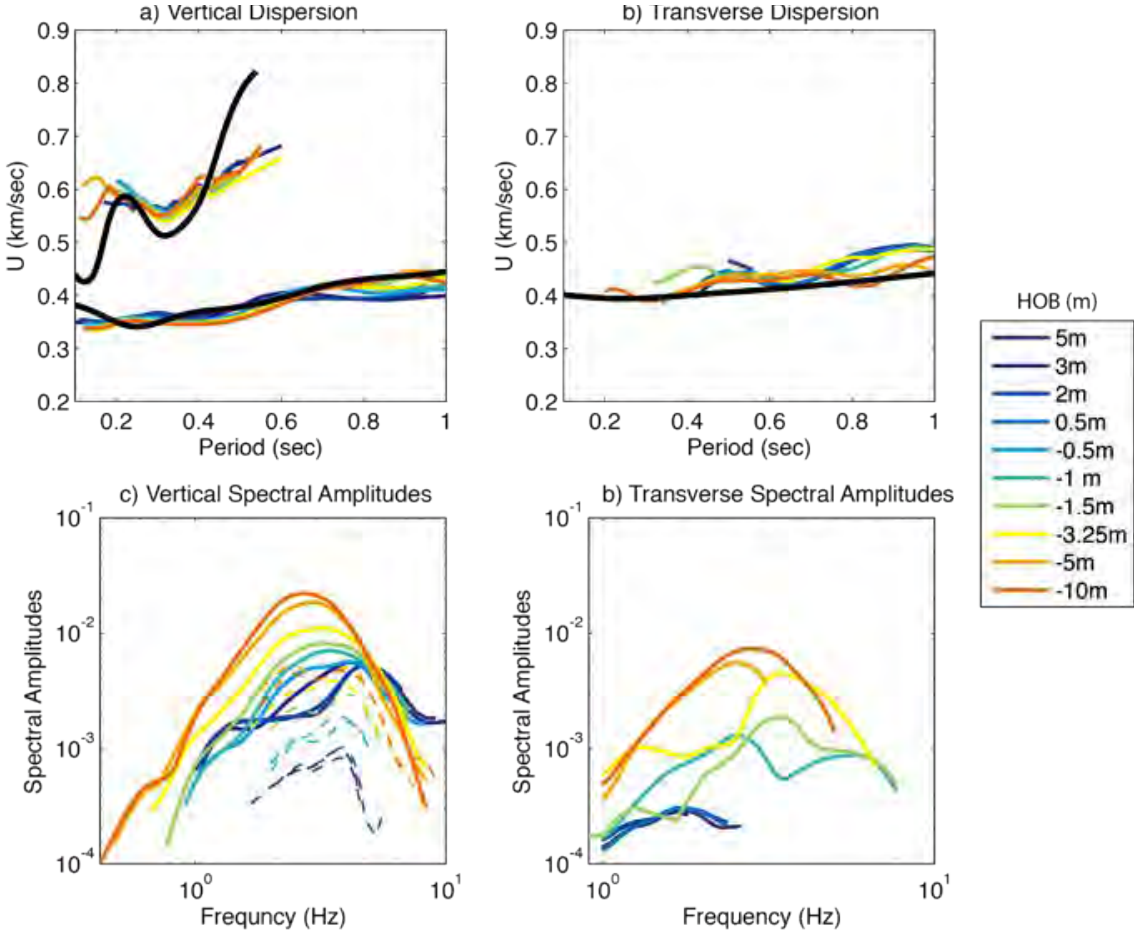

Figure 5. Dispersion and spectra amplitudes for the surface wave phases from all ten 1450-lb HRI and HRII shots. a) HM and FM dispersion. b) *SH* dispersion. c) Spectral amplitudes for FM (solid) and HM (dashed) Rayleigh. d) Spectral amplitudes for the SH. The dispersion curves for the test site velocity model are shown as thick black lines in a) and b).

P/S Ratios

At regional distances, *P/S* ratios have been shown to be a successful discriminant in the frequency range of 6-8 Hz when magnitude, distance, and amplitude corrections (MDAC) are applied. We have examined the *P/S* discriminant at regional and local distances for simultaneously-detonated chemical explosions conducted for the Non-Proliferation Experiment (NPE), Source Phenomenology Experiments in Arizona (SPE Black Mesa and Morenci), Alaska Frozen Rock Experiments (FRE Frozen and Unfrozen), and the New England Damage Experiment (NEDE). These shots were conducted at various scaled depths of burial in lithology ranging from granite to alluvium. Several of these datasets have delay-fired mining explosions detonated in close proximity to the dedicated shots for comparison. During the past year, we have added additional datasets to our analysis of *P/S* ratios from the HRI and HRII explosions.

Phase ratio discriminants at regional distances often compare discrete phases such as *Pn, Pg, Sn*, and *Lg*. This is very difficult to accomplish at local distances due the crossover distance, the distance at which *Pg*

and *Pn* arrive at the same time. This distance generally occurs between 110 and 130 km. The phase arrivals overlap at wider range of distances though, making discrete phase analysis very difficult.

The ratios were examined for dedicated explosions ranging in size from 200 lbs. to 2.7 kt and occurring in different types of lithology varying from ~~"s~~oft" alluvium to ~~"h~~ard" granite. The delay-fired mine blasts were detonated in limestone and granitic porphyry and were recorded as part of the Source Phenomenology Experiments in Arizona (SPE). Ratios were also obtained from earthquakes occurring in the Albuquerque Basin and recorded at local distances.

Individual Station Ratio Discrimination. The analysis initially focused on examining *P/S* ratios on an individual station basis. After determining the appropriate length of the *P* and *S* phase windows, spectral amplitudes were obtained for each phase and a ratio was calculated in a selection of frequency bands. Figure 6 shows an example of the processing and resulting *P/S* spectral ratio for a HRI explosion. Note that the *P* and *S* waves have a different corner frequency and it is this difference that is believed to allow discrimination to work at regional distances. Observation of the corner frequency difference at local distance shows promise for the discriminant to also work at the shorter distances.

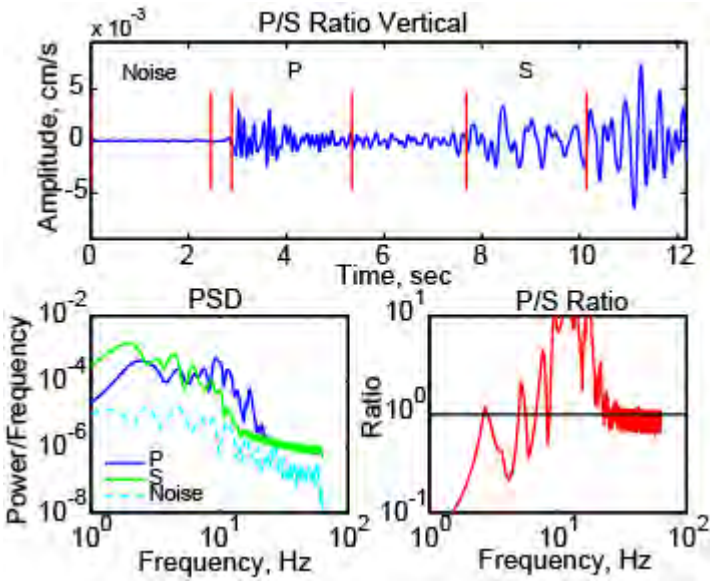

Figure 6. *P/S* spectral ratio calculation of an explosion in the Albuquerque Basin. The top panel shows the data windows from which the spectra were calculated. The bottom left panel shows the spectra of each window and the bottom right panel plots the *P/S* ratio as a function of frequency.

The *P/S* spectral ratios were calculated for all explosions, mine blasts, and earthquakes in frequency bands of 1-2, 2-4, 4-8, and 8-16 Hz. As expected, ratios between 1 and 4 Hz showed no discrimination capabilities. Discrimination begins to take place above 4 Hz as shown in Figure 7. Between 4 and 8 Hz, the explosion ratios fall near the top of the earthquake ratio cloud, although there is still overlap. In addition, at distances less than 50 km, the discrimination appears to break down completely as there is considerable ratio scatter.

It was hypothesized that increasing the frequency band for the ratio calculation for small chemical explosions at local distances would improve the capability of *P/S* ratio discriminants. Figure 7 also shows the ratios between 8 and 16 Hz. The ratios discriminate as well or better at the higher frequency range, but there is limited data due to increased signal attenuation at the higher frequencies. This occurs even for the very large explosions, which also typically have lower corner frequencies.

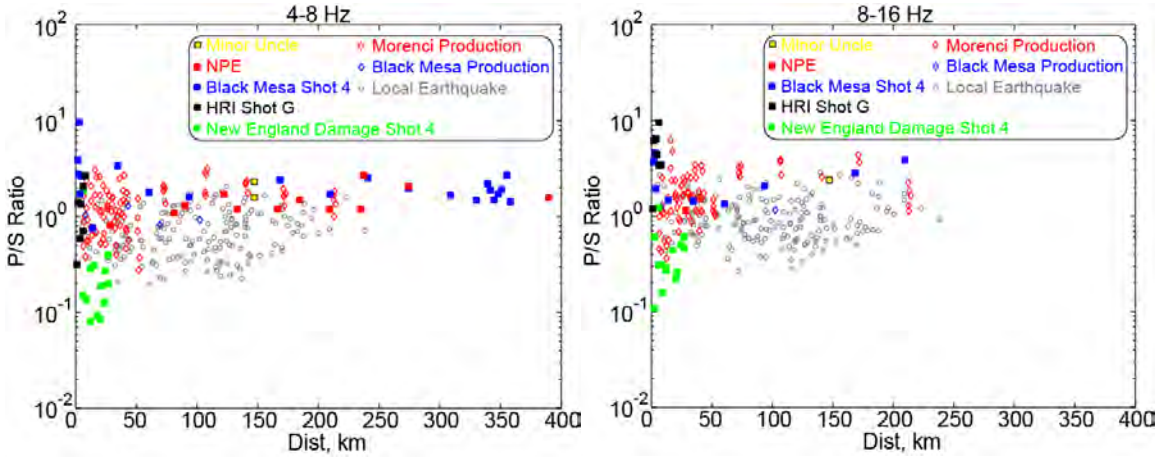

Figure 7. *P/S* spectral ratios of individual stations as a function of distance between (left) 4 and 8 Hz and (right) 8 and 16 Hz.

Network Average Ratio Discrimination. It is often observed that averaging a parameter, such as a phase ratio, across a local network will result in more stable values and improved results. For this portion of the study, the *P/S* ratios calculated for individual stations were averaged across the recording network for each event. This resulted in significantly improved discrimination results and will likely serve as an effective method of discriminating events at local distances (Figure 8).

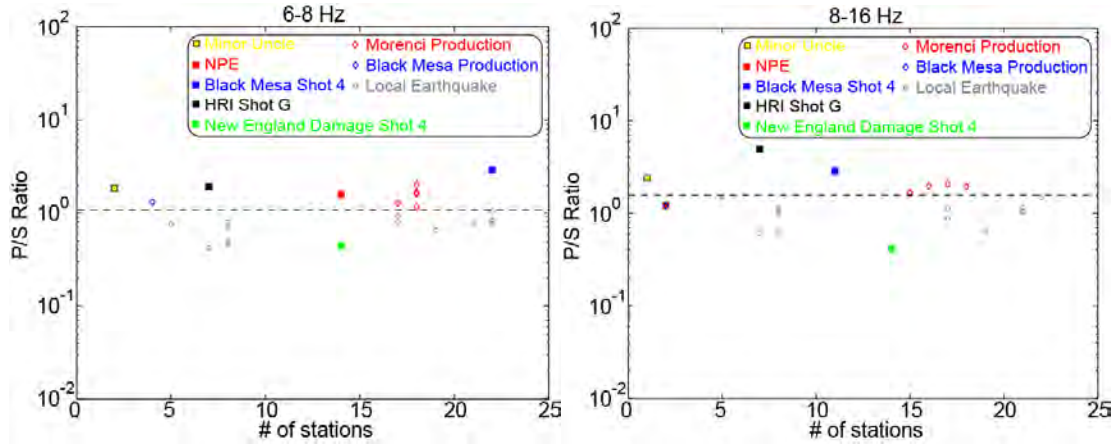

Figure 8. Network averaged *P/S* spectral ratios as a function of the number of stations in the average between (left) 6 and 8 Hz and (right) 8 and 16 Hz.

CONCLUSIONS AND RECOMMENDATIONS

We continue to examine the possible mechanisms for the *S*-wave phase generation for the HUMBLE REDWOOD explosions. The relative amplitude differences between the Rayleigh and Love waves are similar to differences noted for nuclear explosions where Love waves are generated by tectonic release. However, tectonic release does not seem to be a viable mechanism for these small shots in alluvium. Other possible sources for the Love waves include topographic/structural scattering of the Love waves, *pS* conversions at the free surface, and damage and cracking. The topography between the test site and western stations is essentially flat (< 5 m variation), therefore it is highly unlikely that topographic scattering is the source of these Love waves. The largest structural feature that could lead to significant scattering of the *Rg* into Love waves is a fault 2 km to the east of GZ, which would not provide the fit to the observed Love wave travel times. It also seems unlikely that *P* to *S* conversion at the free surface is the source of the

S-waves considering that we have both underground and above ground explosions that appear to be generating Love waves, although it is more difficult to positively confirm *SH* motion on the above ground explosions. We plan to study high speed video of the blasts that show crack development for the blasts as a possible *S*-wave generation mechanism. Finally, we hope to compare WPP modeling currently being completed by Rodgers and Xu to the observed *S*-waves.

ACKNOWLEDGEMENTS

We wish to thank Al Leverette, Artie Rodgers, Scott Phillips, Aaron Ferris, and Hans Hartse for their assistance with the HUMBLE REDWOOD data and research. We thank Dr. Eli Baker for discussion regarding *SH* wave generation from small explosions. We thank Mr. Jim Lewkowicz for his continued support and thoughtfulness. We also thank Artie Rodgers and Hemming Xu for information gleaned from personal communications concerning WPP modeling.

REFERENCES

Dziewonski, A., S. Bloch, and M. Landisman (1969). Surface wave ray tracing azimuthal anisotropy: a generalized spherical harmonic approach technique for the analysis of transient seismic signals, *Bull. Seismol. Soc. Am*., 59: 427–444.

Foxall, B. R., R. Reinke, C. Snelson, D. Seastrand, R. Marrs, O.R. Walton, and A.L. Ramirez (2008). The HUMBLE REDWOOD Seismic/acoustic coupling experiments. Abs. *Seism. Res. Letts*, 79.

Foxall, B, R. Marrs, E. Lenox, R. Reinke, D. Seastrand, J. Bonner, K. Mayeda, and C. Snelson (2010). The HUMBLE REDWOOD seismic/acoustic coupling experiments. Joint inversion for yield using seismic, acoustic, and crater data. Abs. *Seismological Research Letters* 81, No. 2 on page 315.

Hartse, H. E., S. R. Taylor, W. S. Scott, and G. E. Randall (1997). A preliminary study of regional seismic discrimination in central Asia with emphasis in western China, *Bull. Seismol. Soc. Am*., 87: 551–568.

Herrmann, R. B. (2010). *Computer Programs in Seismology*: Version 3.35. St. Louis University.

Lenox, E. A., P. H. Thompson, R. W. Henny (2008). Applicaton of photogrammetric techniques to crater measurements for shallow buried, surface, and small height of burst explosions. Proceedings of the MABS 20 (International Symposium on the Miltary Applications of Blast and Shock) Oslo, Norway, Sept, 2008.

Marrs, R .E., R. Reinke, D.C. Templeton, W. Foxall, E. Lenox, K. Mayeda, J. Bonner, D. Seastrand, and A. Rodgers (2011). Local to near-regional seismic and acoustic signals from fully contained, cratering and height of burst explosions. Abstract. *Seism. Res. Lets.*

Murphy, J. R., H. K. Shah, and T. K. Tzeng (1982). Analysis of low frequency ground motions induced by near-surface and atmospheric explosions, Final Technical Report to Defense Nuclear Agency, DNA-TR-81-157, Alexandria, Virginia.

Pasyanos, M. E. and W .R. Walter (2009). Improvements to regional explosion identification using attenuationmodels of the lithosphere, *Geophys. Res. Lett.* in press, doi:10.1029/2009GL038505.

Reamer, S. K. and B. W. Stump (1992). Source parameter estimation for large, bermed surface chemical explosions. *Bull. Seismol. Soc. Am.,* 82: 406–421.

Reinke, R.E. (1978). Surface wave propagation in the Tularosa and Jornada del Muerot basisn, south central new Mexico. Ph.D. Tehsis. Southern Methodist University, Dallas, TX 148 pp.

Taylor, S. R., M. D. Denny, E. S. Vergino, and R. E. Glaser (1989). Regional discrimination between NTS explosions and western U.S. earthquakes, *Bull. Seismol. Soc. Am.,* 79: 1142–1176.

Walter, W. R., K. Mayeda, and H. J. Patton (1995). Phase and spectral ratio discrimination between NTS earthquakes and explosions, part 1: Empirical observations, *Bull. Seismol. Soc. Am*. 85: 1050–1067.